Volume 56
Number 51
28 June 2020
Pages 6895–7052

ChemComm

Chemical Communications

rsc.li/chemcomm

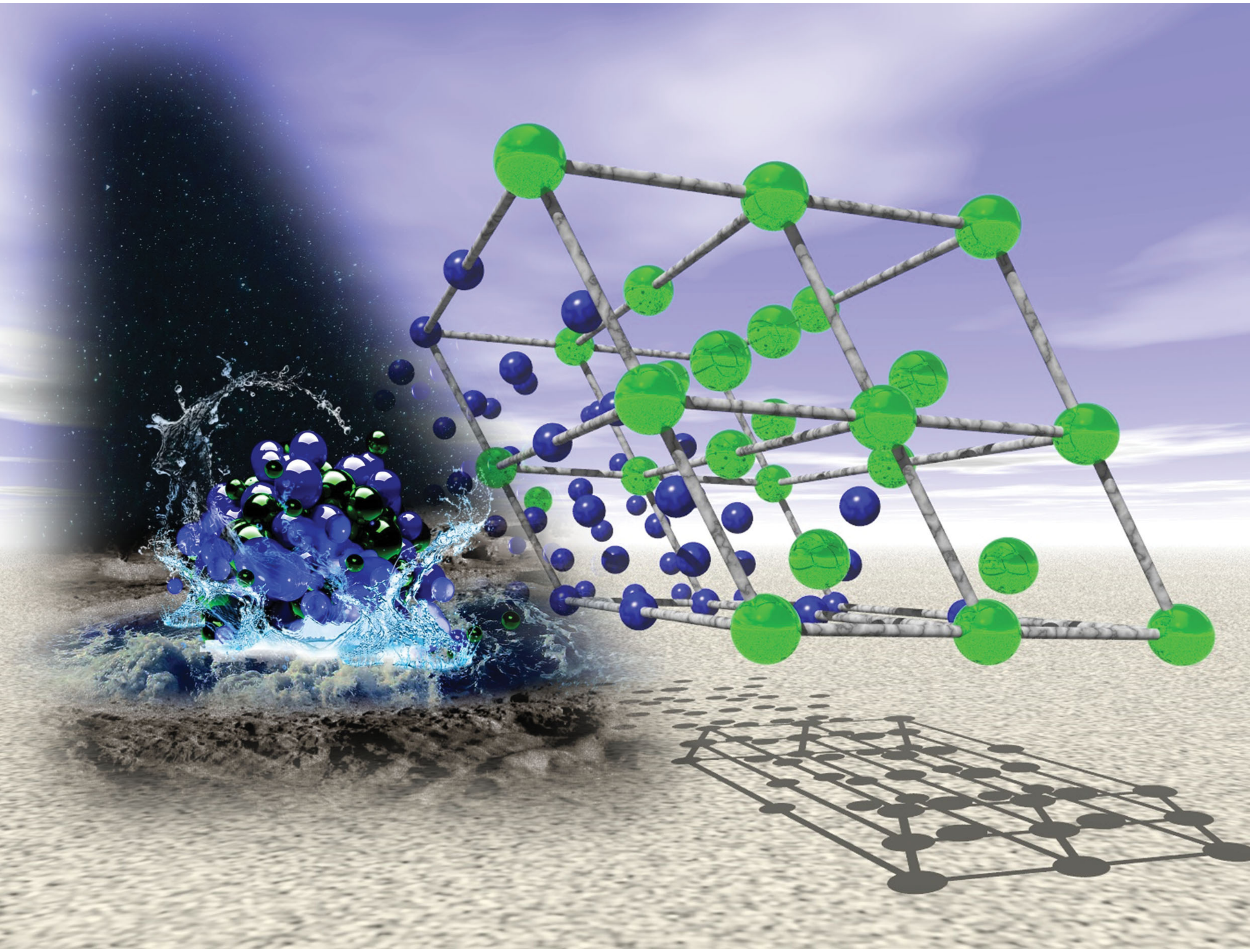

ISSN 1359-7345

ROYAL SOCIETY OF **CHEMISTRY**

COMMUNICATION

Jerry Chun Chung Chan *et al.*

Formation of nano-magnesite in the calcareous spicules prepared under ambient conditions

ChemComm

ROYAL SOCIETY OF CHEMISTRY

COMMUNICATION

View Article Online
View Journal | View Issue

Check for updates

Cite this: *Chem. Commun.*, 2020, **56**, 6925

Received 24th April 2020,
Accepted 21st May 2020

DOI: 10.1039/d0cc02961k

rsc.li/chemcomm

Formation of nano-magnesite in the calcareous spicules prepared under ambient conditions†

Chieh Tsao,‡[a] Pao-Tao Yu,‡[a] Chun-Chieh Wang[b] and Jerry Chun Chung Chan *[a]

We report that high-Mg calcite spherulites can undergo a coarsening process to form calcareous spicules of ~30 microns in width and several hundred microns in length after an aging process in air for a prolonged period. During the aging process, the crystallinity of the calcitic structure has been improved substantially with a significant migration of Mg ions toward the mineral surface. In a thin-foil sample of the spicule aged for 20 months, nanocrystallites of magnesite with minor substitution level of Ca ions have been found near the surface of the spicule.

Spherulites could be prepared in numerous organic and inorganic materials under different crystallization conditions.[1] The preparation of spherulitic calcium carbonates in the presence of Mg^{2+} ions have been well-documented in the literature.[2–6] High-Mg calcites refer to the calcites in which the Mg^{2+} ions in the calcite lattice are higher than 10 mol%.[7] The effects of Mg^{2+} ions on the morphology of calcite and the solution chemistry of the relevant transformation processes have been actively studied.[8–15] Although high-Mg calcite is susceptible to dissolution in aqueous solution, it has been commonly found in the biominerals of marine organisms.[16–19] It is not fully understood why Mg-calcite plays an important role in the process of biomineralization. In addition to its relevance in biomineralization, Mg-calcite is structurally related to magnesite and dolomite, whose formation under ambient conditions is one of the biggest mysteries in geological science. The so-called "dolomite problem" or "magnesite problem" refers to the fact that there is a wealth of evidence in geological science to support the formation of $[Mg,Ca]CO_3$ or $MgCO_3$ in sediments near Earth surfaces, and yet *in vitro* preparation of these anhydrous salts at room temperature has not been successful after decades of efforts.[20] Although low-temperature preparation of anhydrous amorphous magnesium carbonate has been achieved in formamide, Teng and co-workers concluded that the formation of magnesite in water-free environments is thermodynamically unfavorable owing to a substantial entropic hindrance.[21] Nonetheless, the key to the magnesite problem does not necessarily rely on the precipitation of magnesite in a solvent. Herein, we report that calcareous spicules were formed by the coarsening of Mg-calcite spherulites in which nanocrystallites of magnesite were found. The results provided plausible physiochemical rationales on (i) the biological relevance of high-Mg calcite and (ii) the geological formation of magnesite under ambient conditions.

Previously, we reported that spherulites of high-Mg calcite could be prepared in an aqueous solution of L-α-lecithin under ambient conditions, in which mesocrystals of high-Mg calcite were found in the broken fragment of a thin foil of the spherulite.[6] However, to fully characterize the size and orientation of the crystalline domains inside the spherulites, it is highly desirable to obtain an intact thin foil of the spherulite for transmission electron microscopy (TEM) investigations. After repeat attempts, we were able to use focused ion beam (FIB) milling technique[22] to prepare intact thin foils of the spherulites. The samples dried by N_2 flushing are henceforth referred to as S*x*, where *x* denotes the setting time in lecithin solution. The composite bright-field TEM images of S48h are shown in Fig. 1(a). Near the surface of the spherulites, many dark stripes were found aligned radially toward the center. The grayscale of the figure indicates the varying degree to which the impinging electrons had scattered. We acquired the dark-field image originating from the $(10\bar{1}4)$ diffraction spot for the thin foil prepared for S24h (ESI,† Fig. S1). By comparing it with the bright-field image, it was clearly illustrated that the dark-stripe regions comprised well aligned crystallites of calcitic structure. The corresponding selected area electron diffraction (SAED) patterns revealed that the substitution level of Mg in the calcite lattice varied considerably in the length scale of nanometers (ESI,† Fig. S2). To verify whether or not the voids appeared in

[a] *Department of Chemistry, National Taiwan University, No. 1, Section 4, Roosevelt Road, Taipei, 10617, Taiwan. E-mail: chanjcc@ntu.edu.tw*
[b] *National Synchrotron Radiation Research Center, Hsinchu 30076, Taiwan*

† Electronic supplementary information (ESI) available. See DOI: 10.1039/d0cc02961k

‡ Authors contributed equally.

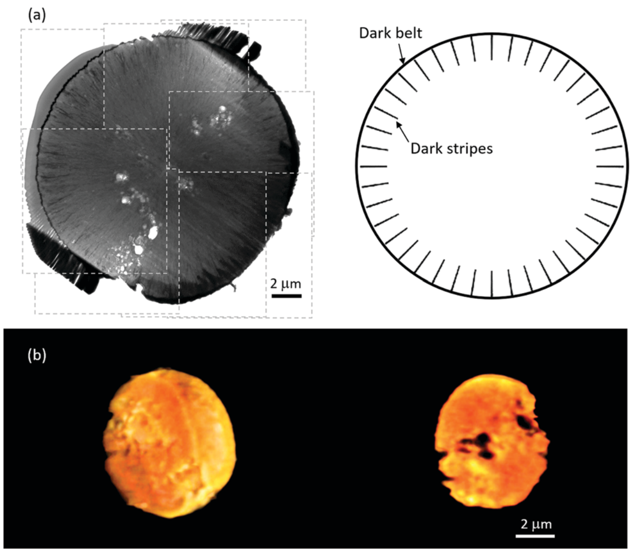

Fig. 1 (a) Composite bright-field TEM image of a thin foil of S48h prepared by FIB. A circular band of dark stripes are prominent in the image. The dark belt was the Pt strap deposited on the sample surface. (b) TXM images of a typical spherulite of the S16h sample. The image on the left shows the exterior of the spherulite, whereas the image on the right is a cross-sectional image taken from the three-dimensional tomograph. The 3D tomograph in mpg file format can be downloaded from the ESI† (Movie S1).

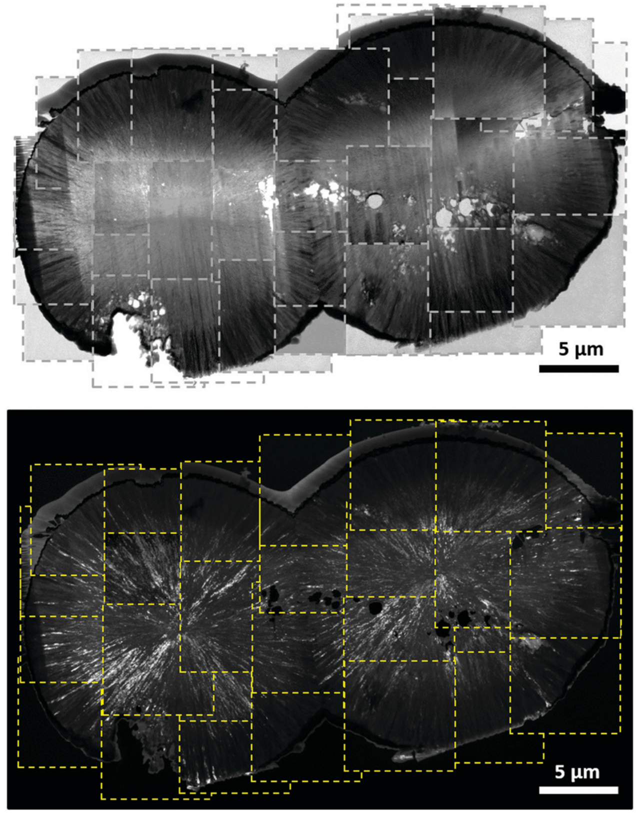

Fig. 2 Composite bright-field TEM image acquired for a twin-spherulite of S48h (upper) and the composite dark-field image of the same particle originating from the (10$\bar{1}$4) diffraction spot (lower).

the bright-field TEM image were artefacts by FIB milling, we acquired the tomographic images of S16h using transmission X-ray microscopy (TXM) with synchrotron radiation sources, from which the micron-sized pores inside the spherulites were clearly observed (Fig. 1(b)).

As illustrated in the SEM image of S16h (ESI,† Fig. S3 and S4), twin-spherulites were found in addition to spherulites. The composite bright-field and dark-field TEM image of a typical twin-spherulite is shown in Fig. 2, where the crystalline stripes of each spherulite were radially aligned such that the center point of each spherulite was well defined. Notably, the dark stripes were not only found on the mineral surface but also in the boundary region of the two hemispherulites, where a sharp boundary was formed (ESI,† Fig. S5). These observations suggested that the twin-spherulite was formed by the fusion of two individual spherulites through the mechanism of contact flattening.[23] To verify whether the spherulites of high-Mg calcite have a strong propensity to fuse together, selected S*x* samples were aged in air under ambient conditions (298 K and 75–80% relative humidity) for different periods of time. The samples are henceforth referred to as S*x*A*y*, where *y* denotes the aging time. With reference to the scanning electron microscopic (SEM) images illustrated in Fig. 3, calcareous spicules up to a length scale of hundreds of microns were formed. For the S28hA2m sample, the spicule appeared to be formed by the fusion of a linear chain of spherulites. The spicule formed for S28hA4m was irregular in width, revealing that the number of fusing spherulites was varied at different spots along the spicule. Interestingly, those spicules found in S28hA12m and S28hA20m were rather uniform in width. The energy-dispersive X-ray (EDX) analysis with SEM showed that the Mg content of

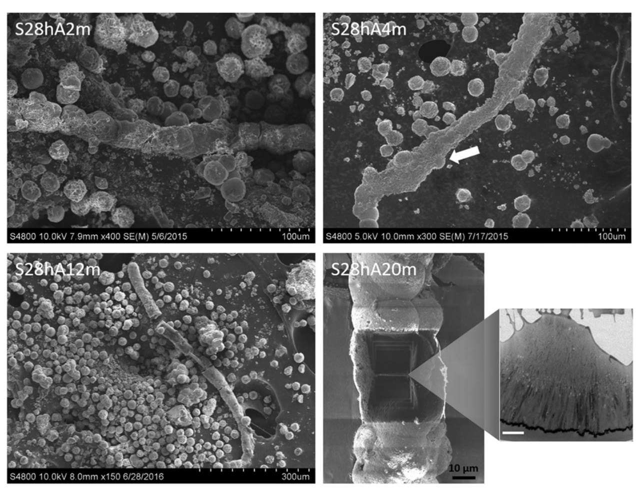

Fig. 3 SEM images of the spicules found in the samples of S28hA2m, S28hA4m, S28hA12m, and S28hA20m. The white arrow in the top-right image indicates the position at which a spherulite fused into the spicule. The width of the spicule was ~30 μm. As shown in the bottom-right image, a thin foil was prepared by FIB for the subsequent TEM imaging. The scale bar in white represents 1 μm.

spherulites was in general on the order of 21% (ESI,† Fig. S6). By contrast, the Mg content measured on the spicule surface was as high as 48% (ESI,† Fig. S7). We inferred that the spicules were formed by the accretion of the high-Mg calcitic spherulites, which was accompanied with a substantial increase in the Mg content on the spherulite surface owing to phase separation. This observation is consistent with the findings that the distribution of Mg^{2+} and Ca^{2+} was rather heterogeneous in biominerals.[24–26] In any case, the pathway of the spicule formation illustrated here is presumably different from that of the calcareous spicule fabricated in the presence of silicatein-α, which is a protein extract of sponges.[27]

A thin foil of the spicule in S28hA20m was prepared for TEM study. Fig. 4 shows the bright-field image of the foil, in which the feature of dark stripes near the mineral surface was again observed. Furthermore, we were able to assign the SAED patterns acquired at different spots with reference to a calcitic structure. Because calcite and magnesite are structurally isomorphic,[28] the Mg content in Mg-calcite can be estimated from the *d*-spacing of $(10\bar{1}4)$ relative to that of calcite or magnesite as long as the structural scenario of solid-solution is justified.[29,30] In the literature, the *d*-spacing of the characteristic $(10\bar{1}4)$ diffraction of magnesite and calcite are reported to be 0.27412 and 0.30357 nm, respectively.[28] For S28hA20m the SAED patterns acquired were analyzed by the diffractGUI software.[31,32] Remarkably, the results of the *d*-spacing of $(10\bar{1}4)$, which ranged from 0.2757(1) to 0.3019(1) nm, revealed that the substitution level of Mg in the calcitic lattice varied from the regime of low-Mg calcite to a level

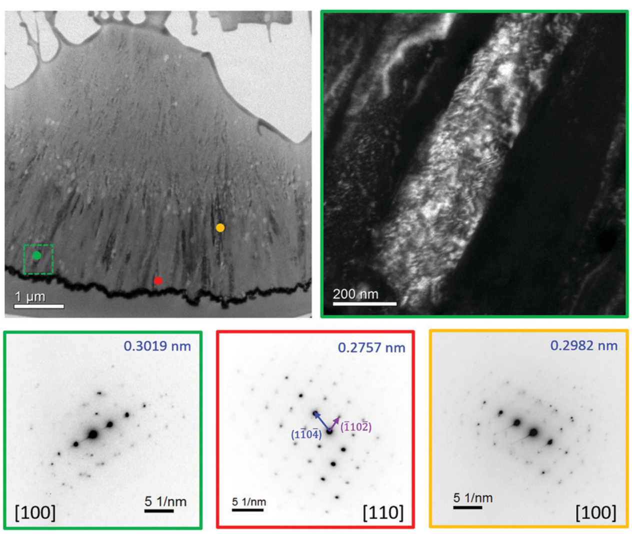

Fig. 4 Bright-field TEM image of the thin foil of S28hA20m and some selected SAED patterns. The top-right image is the dark-field image of a selected region of the bright-field image as indicated by a dashed square in green, where a stripe of mesocrystal of Mg-calcite, which comprised a large collection of well aligned nanocrystallites was observed.[37,38] The SAED patterns of different color frames, taken for a circular area of ~200 nm in diameter, correspond to the regions indicated by the spots of the same color in the bright-field image. The *d*-spacing of $(10\bar{1}4)$ was shown in the top-right corner of each SAED pattern. The large variation in the *d*-spacing cannot be arised from the effect of miscalibration. The SAED pattern in red frame, which was obtained near the spicule surface, resembled closely to that of magnesite. From the scenario of solid-solution, the Mg content was estimated to be ~95%.

that was almost the same as magnesite. Because the XRD pattern of S28hA20m did not contain any characteristic diffraction peak of magnesite, we therefore inferred that only a tiny amount of nanocrystallites of magnesite were formed near the mineral surface of S28hA20m. At the present stage, we only found nanocrystallites of magnesite in the spicules of S28hA20m. Repeat experiments confirmed that spicule formation occurred for S20hA1m, S28hA3m, and S3dA2m (ESI,† Fig. S8), but not for S4hA7m. In other words, the setting time of our samples in lipid solution may be an important factor for the subsequent spicule formation under aging conditions. Because the crystallinity associated with the SAED patterns of S28hA20m is much higher than that of S24h (ESI,† Fig. S2), we surmised that the fusion of the crystallites, which was accompanied by the diffusion of Mg^{2+} ions, had led to a recrystallization process which was facilitated by the moisture adsorbed on the mineral surface.[33–36]

The formation pathway of calcareous spicule revealed in this study may shed considerable insight into the biological relevance of high-Mg calcite. The shell wall of many marine foraminifera forms a primary calcite layer to delineate the boundary of a new chamber.[18] This process, as exemplified in porcelaneous foraminifera, proceeds by assembling crystallites of high-Mg calcites at the site of chamber formation.[18,39] The choice of high-Mg calcites might originate from their ease of structural fusion, in the presence of lipids or other organic species. On a more general note, one may infer that the transient formation of high-Mg calcite in many calcareous biominerals is not an undesirable transient phase during the phase transformation of biogenic ACC, because the spherulites of high-Mg calcite may serve as versatile building blocks for the formation of skeletal framework. The presence of the nanocrystallites of magnesite in S28hA20m is another remarkable observation because the preparation of S28h and the subsequent aging process were carried out under ambient conditions. It has been well established that the geological regions containing Recent magnesite often go through a pronounced annual cycle of aridity and flooding. Typical examples include the laminated sediment of the Great Salt Lake Desert, the carbonate sediments of the coastal plain along the Persian Gulf at Abu Dhabi, and the Holocene sediments of lakes in the Kiskunság National Park.[20] In the light of this work, this geological field observation appears to be closely associated with the aging process in air required for the formation of magnesite through the phase separation process of high-Mg calcite.

Preparation of high-Mg calcitic spherulites is well documented in the literature. To our great surprise, however, one could obtain calcareous spicules and nano-magnesite by simply aging the Mg-calcitic spherulites under controlled humidity conditions for a prolonged period. Evidence was provided to support that the spicules were formed through the fusion of spherulites. We suggest that the aging process was accompanied by the diffusion of Mg ions to the mineral surface which subsequently led to the formation of nano-crystallites of magnesite. These results aptly illustrated the fascinating structural features of high-Mg calcitic spherulites.

This work was financially supported by the Ministry of Science and Technology (106-2113-M-002-023). The TEM and

SEM measurements were carried out at the Instrumentation Center of National Taiwan University, supported by the Ministry of Science and Technology. We thank C.-Y. Chien and S.-J. Ji for their help in FIB and SEM experiments. We thank H.-R. Chen (College of Engineering, National Taiwan University) for his support in HRTEM measurements. The assistance of C.-Y. Lin and Y.-Y. Yang in TEM and SEM measurements is gratefully acknowledged.

Conflicts of interest

There are no conflicts to declare.

Notes and references

1 A. G. Shtukenberg, Y. O. Punin, E. Gunn and B. Kahr, *Chem. Rev.*, 2012, **112**, 1805–1838.
2 S. L. Tracy, D. A. Williams and H. M. Jennings, *J. Cryst. Growth*, 1998, **193**, 382–388.
3 S. Gayathri, R. Lakshminarayanan, J. C. Weaver, D. E. Morse, R. M. Kini and S. Valiyaveettil, *Chem. – Eur. J.*, 2007, **13**, 3262–3268.
4 J. Hermans, L. André, J. Navez, P. Pernet and P. Dubois, *J. Geophys. Res.: Biogeosci.*, 2011, **116**, G01001.
5 J. W. Xiao and S. H. Yang, *CrystEngComm*, 2011, **13**, 2472–2478.
6 P.-T. Yu, C. Tsao, C.-C. Wang, C.-Y. Chang, C.-H. Wang and J. C. C. Chan, *Angew. Chem., Int. Ed.*, 2017, **56**, 16202–16206.
7 S. Raz, S. Weiner and L. Addadi, *Adv. Mater.*, 2000, **12**, 38–42.
8 K. J. Davis, P. M. Dove, L. E. Wasylenki and J. J. De Yoreo, *Am. Mineral.*, 2004, **89**, 714–720.
9 L. Zhu, Q. Zhao, X. Zheng and Y. Xie, *J. Solid State Chem.*, 2006, **179**, 1247–1252.
10 J. Jiang, M.-R. Gao, Y.-H. Qiu, G.-S. Wang, L. Liu, G.-B. Cai and S.-H. Yu, *CrystEngComm*, 2011, **13**, 952–956.
11 X. Long, Y. Ma and L. Qi, *Cryst. Growth Des.*, 2011, **11**, 2866–2873.
12 W. Sun, S. Jayaraman, W. Chen, K. A. Persson and G. Ceder, *Proc. Natl. Acad. Sci. U. S. A.*, 2015, **112**, 3199–3204.
13 B. Purgstaller, V. Mavromatis, A. Immenhauser and M. Dietzel, *Geochim. Cosmochim. Acta*, 2016, **174**, 180–195.
14 J. Xu, J. Wang, M. Hong and H. H. Teng, *Am. Mineral.*, 2016, **101**, 1104–1112.
15 H. Yang, S. Chai, Y. Zhang and Y. Ma, *CrystEngComm*, 2016, **18**, 157–163.
16 W. D. Bischoff, F. T. Mackenzie and F. C. Bishop, *Geochim. Cosmochim. Acta*, 1987, **51**, 1413–1423.
17 L. Addadi and S. Weiner, *Angew. Chem., Int. Ed. Engl.*, 1992, **31**, 153–169.
18 S. Bentov and J. Erez, *Geochem., Geophys., Geosyst.*, 2006, **7**, 1–11.
19 S. Weiner and L. Addadi, *Annu. Rev. Mater. Res.*, 2011, **41**, 21–40.
20 J. C. Deelman, *Low-temperature formation of dolomite and magnesite*, Compact Disc Publications, Eindhoven, 2011.
21 J. Xu, C. Yan, F. Zhang, H. Konishi, H. Xu and H. H. Teng, *Proc. Natl. Acad. Sci. U. S. A.*, 2013, **110**, 17750–17755.
22 P. J. Heaney, E. P. Vicenzi, L. A. Giannuzzi and K. J. T. Livi, *Am. Mineral.*, 2001, **86**, 1094–1099.
23 R. M. German, P. Suri and S. J. Park, *J. Mater. Sci.*, 2009, **44**, 1–39.
24 D. Vielzeuf, J. Garrabou, A. Baronnet, O. Grauby and C. Marschal, *Am. Mineral.*, 2008, **93**, 1799–1815.
25 Y. Ma, B. Aichmayer, O. Paris, P. Fratzl, A. Meibom, R. A. Metzler, Y. Politi, L. Addadi, P. U. P. A. Gilbert and S. Weiner, *Proc. Natl. Acad. Sci. U. S. A.*, 2009, **106**, 6048–6053.
26 C. Moureaux, A. Perez-Huerta, P. Compere, W. Zhu, T. Leloup, M. Cusack and P. Dubois, *J. Struct. Biol.*, 2010, **170**, 41–49.
27 F. Natalio, T. P. Corrales, M. Panthöfer, D. Schollmeyer, I. Lieberwirth, W. E. G. Müller, M. Kappl, H.-J. Butt and W. Tremel, *Science*, 2013, **339**, 1298–1302.
28 D. Graf, *Am. Mineral.*, 1961, **46**, 1283–1316.
29 K. Chave, *J. Geol.*, 1952, **60**, 190–192.
30 J. R. Goldsmith, D. L. Graf and O. I. Joensuu, *Geochim. Cosmochim. Acta*, 1955, **7**, 212–230.
31 M. Klinger and A. Jäger, *J. Appl. Crystallogr.*, 2015, **48**, 2012–2018.
32 M. Klinger, *J. Appl. Crystallogr.*, 2017, **50**, 1226–1234.
33 J. Ihli, W. C. Wong, E. H. Noel, Y.-Y. Kim, A. N. Kulak, H. K. Christenson, M. J. Duer and F. C. Meldrum, *Nat. Commun.*, 2014, **5**, 3169.
34 F. Konrad, F. Gallien, D. E. Gerard and M. Dietzel, *Cryst. Growth Des.*, 2016, **16**, 6310–6317.
35 M. Farhadi-Khouzani, D. M. Chevrier, P. Zhang, N. Hedin and D. Gebauer, *Angew. Chem., Int. Ed.*, 2016, **55**, 8117–8120.
36 Y.-C. Huang, M. B. Gindele, J. Knaus, A. Rao and D. Gebauer, *CrystEngComm*, 2018, **20**, 4395–4405.
37 H. Cölfen and M. Antonietti, *Angew. Chem., Int. Ed.*, 2005, **44**, 5576–5591.
38 L. Bergström, E. V. Sturm (née Rosseeva), G. Salazar-Alvarez and H. Cölfen, *Acc. Chem. Res.*, 2015, **48**, 1391–1402.
39 S. Bentov and J. Erez, *Geology*, 2005, **33**, 841–844.